Prediction of Cylindrical Shell Response by Statistical Energy Methods

DANIEL D. KANA,* WEN-HWA CHU† AND ROGER L. BESSEY‡
Southwest Research Institute, San Antonio, Texas

The response of a closed cylindrical shell is determined for acoustic excitation which is random in time and correlated in space. Two slightly different formulations of the statistical energy method are utilized to compute shell displacement and interior pressure responses which are compared with measured values in ⅓-octave frequency bands. Structural damping estimates are based on linear viscoelastic theory, parameters for which are empirically determined from experimental data. Various ⅓-octave band averages are defined for computing other frequency-dependent parameters for the system. Good over-all agreement between theoretical and experimental results for shell response is achieved when the nonideal characteristics of the ⅓-octave filters are accounted for. On the other hand, agreement for interior pressure response was less satisfactory. A detailed discussion is given for several possible sources of discrepancy.

Nomenclature

A,A' = total area of cylindrical shell and area of applied excitation pressure, respectively: in^2.
a = radius of tank; in.
B_{rm} = gyroscopic coupling coefficient between the scaled mth shell modal equation and rth air modal equation; rad/sec
c_l = longitudinal wave velocity in shell medium; in./sec
c_0 = sound velocity in the air medium; in/sec
E_3 = total energy of the interior air with center frequency ω per unit bandwidth; (in.-lb)//(rad/sec)
$E_{2AF},E_{2AS},E_{2NR},E_2$ = AF, AS, NR and total energy of the shell per unit bandwidth with center frequency ω; (in.-lb)/(rad/sec)
f_r,f_c = shell ring frequency and coincidence frequency, respectively; Hz
$\hat{G}_{p'p''}$, $\hat{C}_{p'p''}$ = cross-spectral and cospectral density of excitation pressure, for pressure at x' and x'', respectively; (psi)^2/(rad/sec)
I_s = number of s-type shell modes
$I_{2AF},I_{2AS},I_{2NR},I_2$ = number of modes for AF, AS, NR modes and the total number of modes of the shell in $(\omega, \Delta\omega)$
i = $(-1)^{1/2}$
$\langle J_n{}^2\rangle_s$ = average s-type joint acceptance per mode
$k_R(x,\omega)$, $k_I(x,\omega)$ = co and quad pressure cross-correlation factor (nondimensional)
M = total mass of the cylinder; (lb-sec^2)/in.
m,n = axial and circumferential wave number of shell modes (nondimensional)
$N_s(\omega)$, $N_r(\omega)$ = total number of the s-type shell modes and the interior air medium, respectively (nondimensional in $(\omega, \Delta\omega)$
n_3,n_r = number of modes per unit bandwidth for the interior air; (rad/sec)$^{-1}$
$n_{2AF},n_{2AS},n_{2NR},n_2$ = number of modes per unit bandwidth for AF, AS, NR modes and the total number of the shell, respectively; (rad/sec)$^{-1}$
$P_{2s}{}^{IN},P_2{}^{IN}$ = input power to the s-type shell modes and to the shell, respectively, per unit bandwidth with center frequency ω; (in-lb/sec)/(rad/sec)
R = distance on projected area of applied pressure; in.
R_{rad} = radiation resistance; (lb-sec^2)/in./(rad/sec)
r,θ,x = cylindrical coordinates
$S_{p0}(\omega)$ = point reference pressure spectral density; (psi)^2/(rad/sec)
$S_y(\omega)$, $Sp_3(\omega)$ = spectral density of the shell response and interior pressure (in.^{2})/(rad/sec) and (psi)^2/(rad/sec), respectively
s,q = scaled displacement of the shell and the air, respectively; in., unless otherwise defined
V_3,V = volume of the interior air; in.^{3}
$\underline{x},\underline{x}',\underline{x}''$, $\underline{x}_1,\underline{x}_2$ = two-dimensional position vectors on shell surface, e.g., specified by (a, θ_1, x_1), etc.
Z_m,Z_r = impedance of the mth shell mode and rth air mode, respectively; (rad/sec)^2
α_k = kth input power correction factor; (nondimensional)
β_m,β_r or β_{mn},β_{rst} = damping coefficient of the mth shell mode and rth air mode, respectively; rad/sec or that of the mnth shell mode and rstth air mode
δ_{mn},δ_{rk} = Kronecker delta; unity when $m=n$ or $r=k$, otherwise zero
η_2,η_3 = loss factor in shell and in the interior air, respectively; (nondimensional)
η_{23s},η_{21s} = coupling loss factor between shell and interior air and that between shell and exterior air, respectively, for the s-type mode
υ_e = Poisson's ratio for elastic shell
υ_v = Poisson's ratio for viscoelastic shell
ρ_0 = density of the air medium; (lb-sec^2)in.^{4}
$\rho_s h_s$ = mass per unit area of the shell; (lb-sec^2)/in^3.
ϕ_m,ψ_r = mth shell normal mode and rth air normal mode
ϕ_{mn},ω_{mn} = shell normal mode and natural frequency of mth and nth axial and circumferential wave number, respectively; nondimensional and rad/sec, respectively.
ψ = a generalized fluid displacement
ω_m,ω_r = mth and rth shell and air natural frequencies, respectively; rad/sec
l,h = length and width of an "equivalent rectangular" plate for the shell

Subscripts and Supercripts

$\langle\ \rangle$ = time average
$(\ )s$ = $s = AF$, AS, NR modes, respectively, or for the shell when $(\ )$ is the same for all these modes
$(\omega,\Delta\omega)$ = frequency band centered at ω of bandwidth $\Delta\omega$
$(\hat{\ })$ = amplitude of $(\ )$
$(\dot{\ })$ = time derivative of $(\ )$
$(\ )m$ = $(\ )$ related to the mth shell mode
$(\ )r$ = $(\ )$ related to the rth air mode
$(\ )^*$ = complex conjugate of $(\ )$
$(\ )^{\langle\varpi,\Delta\varpi\rangle}$ = average over $(\omega, \Delta\omega)$
$(\tilde{\ })$ = Fourier transform of $(\ )$

Presented as Paper 71-331 at the AIAA/ASME 12th Structures, Structural Dynamics and Materials Conference, Anaheim, Calif., April 19–21, 1971; submitted May 13, 1971; revision received November 1, 1971. The results presented in this paper were obtained during the course of research sponsored by NASA Marshall Space Flight Center under Contract NAS8-21479.

Index category: Structural Dynamic Analysis.

* Manager, Structural Dynamics and Acoustics, Department of Mechanical Sciences. Member AIAA.

† Staff Scientist, Department of Mechanical Sciences. Member AIAA.

‡ Research Engineer, Department of Mechanical Sciences.

Introduction

DETERMINATION of the response of elastic structures to distributed random pressures is of fundamental concern in many engineering applications. It assumes particular significance in aerospace environments where acoustical energy from several sources exerts a profound influence on the dynamic response of the structure, as well as on its interior components. These pressures are usually random in time, have a spatial cross-correlation which is dependent on the phase of the launch trajectory, and in general, cannot be simulated by a diffuse field.

Various methods are available for the prediction of structural response to random excitation. Of these, the modal method is generally considered to be useful in low-frequency regions which include low-modal density. Some of its limitations for application to the case of a cylindrical shell excited by random acoustic excitation were determined in the initial phase[1] of the present program. The results of the remaining work, which are reported herein,§ represent an investigation of the response of the same basic cylindrical configuration over much wider frequency ranges which include high-modal density and significant acoustic radiation. Two different formulations of the statistical energy method are employed for prediction of response. In previous work, use of this method has generally been reserved to applications in which the loading is a diffuse pressure field. Our purpose is to determine its applicability to a case where a high degree of spatial correlation exists.

Experimental Analysis

In order to provide a relatively simple nondiffuse excitation, the physical arrangement depicted in Fig. 1 was selected. This is a similar system to that which was utilized in our previous effort,[1] except that more elaborate calibration procedures are necessary at higher frequencies, and the cylinder was capped in this case. The acoustical speaker was chosen to provide a reasonably effective area of excitation, yet small enough to minimize the computations required to obtain theoretical numerical results. The entire apparatus, which was designed to perform several related experiments, was composed of six parts: test fixture, excitors, excitation sources, transducers, analyzers, and recording devices, all of which are shown in the schematic of Fig. 2.

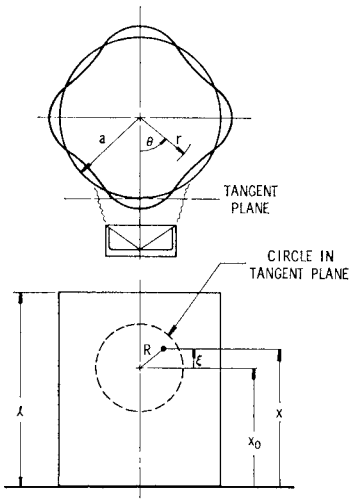

Fig. 1 Coordinate system.

The test structure was a thin-walled aluminum cylinder whose physical properties are given in Table 1. The primary exciter was an 8-in. "hi-fi" loudspeaker which was mounted in relation to the cylinder as described by the coordinate system in Fig. 1, where $x_0 = 15.00$ in. The plane defined by the edges of the speaker cone was parallel to and 0.85 in. from the tangent plane to the cylinder at the excitation center $(r, \theta, x = a, 0, x_0)$.

Five transducers were used to measure characteristics of the cylinder under excitation. Three of these were Bentley displacement detectors located relative to coordinates of Fig. 1,

Table 1 Properties of test cylinder

$\rho_s = 2.59 \quad 10^{-4}$ lb-sec^2/in^4	$l = 30.0$ in.
$h_s = 0.020$ in.	$f_r = 2{,}640$ Hz
$a = 12.42$ in.	$f_c = 23{,}300$ Hz
Material = 6061-T6 Aluminum	

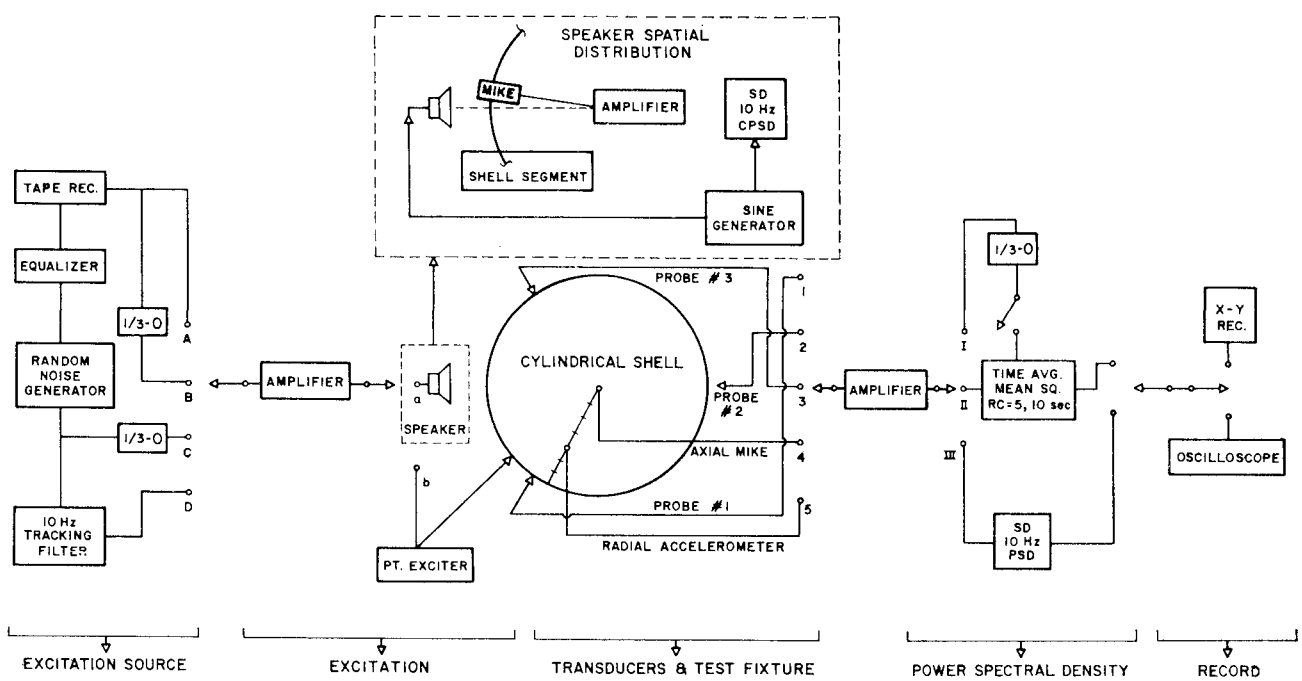

Fig. 2 Schematic of instrumentation.

§ Further details of both experimental and theoretical analyses can be obtained from Ref. 2, from which this paper was condensed.

Table 2 Transducer locations

	θ	x
Probe 1	81°	7.55 in.
Probe 2	204°	12.25 in.
Probe 3	318°	24.40 in.

values for which are given in Table 2. A fourth transducer was a B&K ¼-in.-diam microphone located at various points inside the cylinder. The fifth transducer was an Endevco acclerometer located on the top plate of the test fixture at various points along a radius at $\theta = 45°$. Transducer signals were amplified and analyzed by three analog methods as shown in Fig. 2.

In order to define the spatial correlation of the acoustic field, calibrations were performed on the speaker prior to its use in the experiments. The instrumentation setup for the speaker calibration is seen in block diagram form (within the dashed-line area) in Fig. 2, and is described in detail in Ref. 1. Mapping of the acoustic field spatial correlation was done for the center frequencies of the ⅓-octave filters only, and was thus considered to be an average over each respective band. The field was found to be essentially symmetric with the axis of the speaker cone; thus, only one coordinate (R in Fig. 1) was necessary to designate a point located in the tangent plane, but coincident with a point on the shell at which the sound pressure was measured with the microphone.

In order to obtain the field distribution, a cross-spectral density was computed between the pressures measured at $R = 0$ and those for various $R \neq 0$. These data were found to consist of real (CO) and imaginary (QUAD) parts, and were completely correlated in space as was expected. Data were taken relative to CO of CPSD = 1.0 for $R = 0$. The general empirical equation

$$k_R = \exp(-A_0 R^{B_0}) \cos(\pi R/P_0) \tag{1}$$

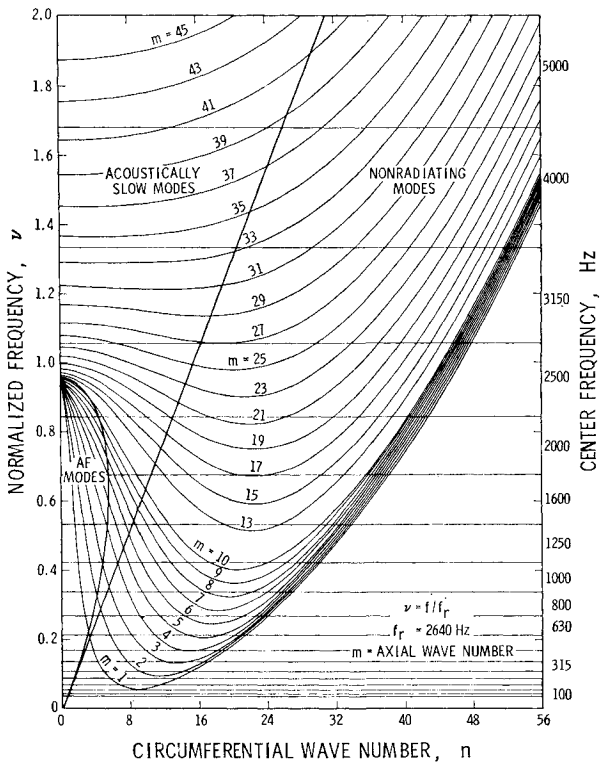

Fig. 3 Modal diagram for cylindrical shell.

was found to fit the CO data well for various values of A_0, B_0, and P_0, which were dependent on the center frequencies of the ⅓-octave filters. The empirical equation

$$k_I = D_0 \cos(\pi R/G_0) - B_0 \tag{2}$$

fit the data for the QUAD part where the constants D_0, E_0, and G_0 also were dependent on the center frequencies of the ⅓-octave filters. Values of these parameters for various center frequencies can be determined from the relative CO and QUAD plots given in Ref. 2.

In order to provide a complete absolute calibration of the speaker field, the preceding relative distribution must be combined with a power spectral density measurement at $R = 0$. Three methods were utilized for this measurement, as indicated in Fig. 2. The experiments involved measurements of shell displacement and interior air pressure response for the following conditions (see Fig. 2 for switch positions). 1) Wide-band equalized excitation source—the loudspeaker was used as the exciter, and the output of the proximity probes was analyzed with the ⅓-octave filters (switch locations *A*, *a*, 1–4, I) and the Ballantine meter. 2) One-third-octave equalized excitation source—the loudspeaker was used as the exciter, and the output of the proximity probes was analyzed with the Ballantine meter directly (switch locations *B*, *a*, 1–4, II). 3) One-third-octave nonequalized excitation source the loudspeaker was used as the exciter, and the output of the proximity probes was analyzed with the Ballantine meter directly (switch locations *C*, *a*, 1–4, II).

Theoretical Analysis

General Modal Relationships

Before proceeding to discuss the details of the statistical energy method as applied to the vibration of a cylinder in air, first it is necessary to recognize the existence of different modal groups over various parts of a wide frequency band. Some of the principles set forth by Manning and Maidanik[3] will be utilized for this purpose.

Figure 3 shows a diagram which depicts many of the modes of the present cylinder over a wide frequency range. The general relationship utilized for calculating these modes is

$$\nu = \{\beta_0^2 a^4[(n/a)^2 + (m_0\pi/l)^2]^2 + (1 - \nu_e^2)(m_0\pi/l)^4/[(n/a)^2 + (m_0\pi/l)^2]^2\}^{1/2} \tag{3}$$

where

$$\nu = f/f_r, \quad \beta_0^2 = h_s^2/(12a^2), \quad m_0 = m + 0.2$$

$$f_r^2 = c_l^2/(4\pi^2 a^2), \quad c_l^2 = E/[\rho_s(1 - \nu_e^2)]$$

Note, that following Arnold and Warburton,[4] an effective axial wave number m_0 is utilized for the present case of a cylinder with partially fixed ends.

The modes of the cylinder have been separated into three distinct groups representing nonradiating (*NR*), acoustically slow (*AS*), and acoustically fast (*AF*) modes. Nonradiating and acoustically slow modes are separated by the straight line

$$\nu = (c_0/c_l)n \tag{4}$$

while acoustically slow and acoustically fast modes are approximately separated by the curve

$$n = (c_l/c_0)\nu\, Re\, [\{(1 - \nu_e^2)^{1/2} - \nu[1 - (\nu/\nu_c)^2]^{1/2}\}^{1/2}] \tag{5}$$

where

$$\nu_c = f_c/f_r, \quad f_c = c_0^2/2\pi(D/\rho_s h_s)^{1/2}, \quad D = Eh^3/12(1 - \nu_e^2)$$

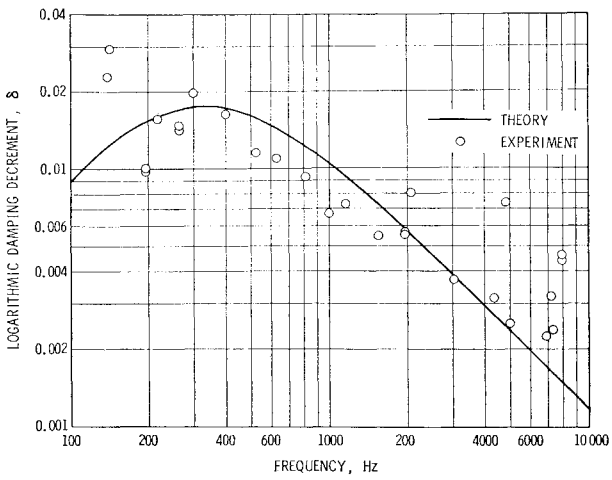

Fig. 4 Damping decrement for cylindrical shell.

Thus, for each $\frac{1}{3}$-octave band, the number of each type of modes I_{2AF}, I_{2AS}, and I_{2NR} were counted directly from Fig. 4, along with Eqs. (4) and (5). It should be recognized that additional acoustically fast modes occur at higher frequencies outside the set range of 5000 Hz.

Power Balance Equations

One possible form of power balance equations for the vibration of a cylinder in air has been presented by Bozich and White.[5] However, their equations do not directly contain terms which allow for a nondiffuse excitation, or for nonradiating modes. Therefore, we will first present a similar set of equations which do account for such additions. These equations will be referred to as the *separate group theory*, for reasons which will become obvious. Then, as a result of discrepancies which resulted between this theory and measured values in part of the frequency range, a second, slightly modified theory is developed. It will be referred to as the *percentage theory*. In particular, the noninteraction between *AF*, *AS*, and *NR* structural modes of the shell is considered in an alternate manner. Both, however, are slightly different modifications of the same basic statistical energy theory.

For our present problem, resonant modes are grouped so that the subscripts 1–3 are used for the outside air, the cylindrical shell, and the interior air, respectively. However, group 2 is further separated into *NR*, *AS*, and *AF* modes. In the separate group theory, essentially five groups are then defined, i.e., 1, 2*NR*, 2*AS*, 2*AF*, and 3. In this case, we may write power balance (per unit bandwidth) equations for the cylinder.

$$\omega\eta_2 E_{2AF} + \omega\eta_{23AF} n_{2AF}\left(\frac{E_{2AF}}{n_{2AF}} - \frac{E_3}{n_3}\right) + \omega\eta_{21AF} n_{2AF}\frac{E_{2AF}}{n_{2AF}} = P_{2AF}{}^{IN} \quad (6)$$

$$\omega\eta_2 E_{2AS} + \omega\eta_{23AS} n_{2AS}\left(\frac{E_{2AS}}{n_{2AS}} - \frac{E_3}{n_3}\right) + \omega\eta_{21AS} n_{2AS}\frac{E_{2AS}}{n_{2AS}} = P_{2AS}{}^{IN} \quad (7)$$

$$\omega\eta_2 E_{2NR} = P_{2NR}{}^{IN} \quad (8)$$

Note that for nonradiating (*NR*) modes the acoustic coupling is considered negligible. Similarly, for the interior air

$$\omega\eta_3 E_3 - \omega\eta_{23AF} n_{2AF}\left(\frac{E_{2AF}}{n_{2AF}} - \frac{E_3}{n_3}\right) - \omega\eta_{23AS} n_{2AS}\left(\frac{E_{2AS}}{n_{2AS}} - \frac{E_3}{n_3}\right) = 0 \quad (9)$$

Now, consider a slightly alternate method of arranging the governing equations. Consistent with the concepts of the statistical energy theory, the modes of each separate medium (1 or 2 or 3) are assumed to possess approximately the same energy level. In particular, we shall assume that the shell structural modes, *AF*, *AS*, or *NR* are approximately of the same energy so the structural coupling between these modes can be neglected. We have

$$E_2/n_2 = E_{2AF}/n_{2AF} = E_{2AS}/n_{2AS} = E_{2NR}/n_{2NR} \quad (10)$$

Since the exterior domain of air is assumed to be of nearly infinite extent, there is only radiation outward from the shell with negligible reflected radiation. The power equation of medium 1 thus is decoupled from the shell-interior-air power equations. We then have the following average power balance equation (per unit band width) for *AF*, *AS*, and *NR* modes, respectively:

$$\omega\eta_2 E_{2AF} + \omega\eta_{23AF} n_{2AF}\left(\frac{E_2}{n_2} - \frac{E_3}{n_3}\right) + \omega\eta_{21AF} n_{2AF}\frac{E_2}{n_2} = P_{2AF}{}^{IN} \quad (11)$$

$$\omega\eta_2 E_{2AS} + \omega\eta_{23AS} n_{2AS}\left(\frac{E_2}{n_2} - \frac{E_3}{n_3}\right) + \omega\eta_{21AS} n_{2AS}\frac{E_2}{n_2} = P_{2AS}{}^{IN} \quad (12)$$

$$\omega\eta_2 E_{2NR} = P_{2NR}{}^{IN} \quad (13)$$

Similarly, the average power balance equation for the interior air mode is

$$\omega\eta_3 E_3 - \omega\eta_{23AF} n_{2AF}\left(\frac{E_2}{n_2} - \frac{E_3}{n_3}\right) - \omega\eta_{23AS} n_{2AS}\left(\frac{E_2}{n_2} - \frac{E_3}{n_3}\right) = 0 \quad (14)$$

Equations (11–14) are the basic governing equations for the percentage method. Consider now a slight rearrangement of these equations which makes the name of the method more obvious. The total energy of the shell is

$$E_2 = E_{2AF} + E_{2AS} + E_{2NR} \quad (15)$$

The total number of shell resonant modes per unit bandwidth is

$$n_2 = n_{2AF} + n_{2AS} + n_{2NR} \quad (16)$$

Only resonant modes are counted, since except at low frequencies, their contribution to energies outweighs other modes provided that they are lightly damped. If Eqs. (11–13) are summed (with equal weight), one obtains

$$\omega\eta_2 E_2 + \omega\eta_{23} n_2\left(\frac{E_2}{n_2} - \frac{E_3}{n_3}\right) + \omega\eta_{23} n_2\left(\frac{E_2}{n_2}\right) = P_2{}^{IN} = P_{2AF}{}^{IN} + P_{2AS}{}^{IN} + P_{2NR}{}^{IN} \quad (17)$$

where the coupling coefficients are

$$\eta_{2j} = \frac{n_{2AF}}{n_2}\eta_{2jAF} + \frac{n_{2AS}}{n_2}\eta_{2jAS}, \quad j = 1 \text{ or } 3 \quad (18)$$

Equation (18) expresses each part of the radiation as a portion, or percent, of the total radiation. This is similar to that presented by Manning and Maidanik.[3]

The determination of number of modes I_{2AF}, I_{2AS}, I_{2NR} in each given bandwidth $\Delta\omega$ centered at ω is described in the previous section. For the shell, the respective modal densities are then

$$n_{2AF} = I_{2AF}/\Delta\omega, \text{ etc.} \tag{19}$$

For the number of interior air modes, we will employ those for an equivalent rectangular room (which is only an approximation for the present case)

$$n_3 = \omega^2 V_3/(2\pi^2 c_0{}^3) \tag{20}$$

Further,

$$E_3 = \rho_0 V_3 \langle \dot{\psi} \rangle^2/\Delta\omega = S_{p3}(\omega) V_3/\rho_0 c_0{}^2 \tag{21}$$

and

$$E_2 = M\langle y^2 \rangle/\Delta\omega = M\omega^2 S_y(\omega) \tag{22}$$

where y is the space-averaged shell displacement. The space-averaged pressure spectral density of the interior, Sp_3, and the space-averaged shell displacement spectral density, S_y, can be calculated from Eqs. (21) and (22) after E_2 and E_3 are determined from the power balance equations.

Input Power

Previous investigators have usually considered only one dominant form of energy loss in impedance relationships which affect input power expressions. In the present case, where energy losses vary considerably from one part of the frequency range to another, a more accurate approximation will be considered.

The Fourier transform of Eqs. (9.1a) and (9.1b) of Lyon–Maidanik[6] yields

$$\tilde{s}_m + \sum_r^{Nr} \frac{B_{rm}\tilde{q}_r}{Z_m{}^*(\omega)} = \frac{\tilde{F}_m}{Z_m{}^*(\omega)}, \quad \tilde{\dot{s}}_m = -i\omega\tilde{s}_m \tag{23}$$

$$\tilde{q}_r - \sum_m^{Ns} \frac{B_{rm}\tilde{s}_m}{Z_r{}^*(\omega)} = 0 \tag{24}$$

where

$$Z_m(\omega) = \omega_m{}^2 - \omega^2 + i\beta_m\omega, \quad Z_r(\omega) = \omega_r{}^2 - \omega^2 + i\beta_r\omega \tag{25}$$

Using Eqs. (23) and (24), the power input can be expressed as

$$P_s{}^{IN} = \frac{M}{\Delta\omega}\sum_m^{Ns}\langle F_m\dot{s}_m\rangle = \frac{M}{2\pi}\cdot\frac{2}{T}Re\sum_m^{Ns}(\tilde{F}_m{}^*\tilde{\dot{s}}_m)^{\langle\omega,\Delta\omega\rangle}$$

$$= P_{Is}{}^{IN} + P_{IIs}{}^{IN} \cong \frac{P_{Is}{}^{IN}}{1+\alpha_{rad_s}} \tag{26}$$

in which α_{rad} is a radiation correction factor to be determined later, and an "integral approximation" and the residue theorem have been used to evaluate band-average values for a lightly damped system. Note that we have also used

$$(\Delta\omega)\hat{C}_{xy}(\omega) = \langle x(t)y(t)\rangle = \frac{1}{2\pi T}\int_{-\infty}^{\infty}\tilde{x}^*(\omega)\tilde{y}(\omega)d\omega$$

$$\cong \frac{(\Delta\omega)}{2\pi T}[\tilde{x}^*(\omega)\tilde{y}(\omega)^{\langle\omega,\Delta\omega\rangle} + \tilde{x}^*(-\omega)\tilde{y}(-\omega)^{\langle\omega,\Delta\omega\rangle}]$$

$$= \left(\frac{\Delta\omega}{2\pi}\right)\frac{2}{T}Re\,[\tilde{x}^*(\omega)\tilde{y}(\omega)^{\langle\omega,\Delta\omega\rangle}]$$

and

$$P_{Is}{}^{IN} = \frac{M}{2\pi}\cdot\frac{2}{T}Re\sum_m^{Ns}\frac{\tilde{F}_m\tilde{F}_m{}^*(-i\omega)^{\langle\omega,\Delta\omega\rangle}}{Z_m{}^*(\omega)}$$

$$\cong \frac{M}{2\pi T}2\sum_m^{Ns}\tilde{F}_m{}^*\tilde{F}_m\left(\frac{\pi}{2\Delta\omega}\right) \tag{27a}$$

$$\cong \frac{\pi}{2Mm}A^2 n_s\langle J_n{}^2\rangle_s\, S_{p0}(\omega),\ s = AF, AS, NR, \text{ respectively} \tag{27b}$$

The joint acceptance in Eq. (27b) can be derived from Eqs. (27a) as

$$\langle J_n{}^2\rangle_s = \frac{1}{A^2 I_s}\sum_m^{Ns}\int_{A''}\int_{A'}\frac{\hat{C}_{p'p''}}{S_{p0}}\phi_m(\underline{x}')\phi_m(\underline{x}'')d\underline{x}'d\underline{x}'' \tag{28}$$

where

$$p' = p(\underline{x}',t), \quad p'' = p(\underline{x}'',t) \quad I_s = n_s\Delta\omega$$

Now let

$$\hat{G}_{p'p0} = k_R(\underline{x}',\omega)S_{p0}(\omega) - jk_I(\underline{x}',\omega)S_{p0}(\omega)$$

$$= \hat{C}_{p'p0} - j\hat{Q}_{p'p0} \tag{29}$$

Then, it can be shown (Ref. 2) that

$$\hat{C}_{p'p''} = Re\,\hat{G}_{p'p''} = [k_R(\underline{x}',\omega)k_R(\underline{x}'',\omega) + k_I(\underline{x}',\omega)k_I(\underline{x}'',\omega)]S_{p0}(\omega) \tag{30}$$

Returning to the correction factor in Eq. (26) with the help of Eqs. (23) and (24), we have for $N_s \neq 0$ (all terms are zero when $N_s = 0$)

$$\alpha_{rad} = \left\{Re\left[\sum_m^{Ns}\tilde{F}_m{}^*\tilde{\dot{s}}_m{}^{\langle\omega,\Delta\omega\rangle}\right]\right\}^{-1} \times Re\left\{\sum_m^{Ns}\sum_r^{Nr}\frac{B_{rm}\tilde{q}_r\tilde{F}_m{}^*(-i\omega)}{Z_m{}^*(\omega)}\right\}^{\langle\omega,\Delta\omega\rangle} \tag{31}$$

Again, from integral approximation, but summing first with respect to r in a procedure entirely analogous to that for Eq. (11-1) of Lyon and Maidanik,[6] the first double sum in Eq. (31) is

$$\alpha_m = (\pi/2)\,R_{rad}/\Delta\omega M \Rightarrow (\pi/2)\,(\omega/\Delta\omega)(\eta_{23} + \eta_{21}) \tag{32}$$

Thus, we can say

$$\alpha_{rad} = \sum_k^{Ns}\alpha_k \tag{33}$$

For $N_s \neq 0$, the minimum possible value of α_k may be α_m while the maximum possible value may be $N_s\alpha_m$. As an estimate of the correction for later discussion, we shall use

$$1 + \alpha_{rad\ AF} \cong 1 + [(N_s + 1)/2]\alpha_m = 1 + (I_{2AF} + 1)/2\,(\omega/\Delta\omega)(\eta_{23AF} + \eta_{21AF})\pi/2 \tag{34}$$

Note that α_{rad_s} is negligible for other than acoustic fast modes.

Coupling Factors

The radiation coefficient for AF modes is approximately[3]

$$R_{21AF} = R_{23AF} = R_{rad\ AF} = \rho_0 c_0 A \tag{35}$$

For acoustically slow modes[2,7,8]

$$R_{rad\ AS} = A\rho_0 c_0\{2\alpha^2(\lambda_a\lambda_c)G_1(f/f_c) + (P_r\lambda_c/A)G_2(f/f_c)\}$$

for $k_p > k_a$, i.e., $c_p < c_0$ or AS modes (36)

where, in our case, the perimeter of an equivalent plate is

$$P_r = 4\pi a + 2l \tag{37}$$

As pointed out by Crocker and Price[8] Eq. (36) applies for AS modes which are edge modes, thus proportional to its effective edge. The resistance for radiation from the cylindrical shell to the exterior through AS modes is then[2,9]

$$R_{21AS} = R_{\text{rad } AS}^{3/4 \text{ space}} = \tfrac{2}{3} R_{AS}^{1/2 \text{ space}} = \tfrac{2}{3}\left(\frac{2\pi a}{2\pi a + 2l}\right) R_{\text{rad } AS} \tag{38}$$

Similarly, the resistance for radiation from the cylindrical shell into the interior through AS modes is

$$R_{23AS} = R_{\text{rad } AS}^{1/4 \text{ space}} = 2R_{AS}^{1/2 \text{ space}} = 2\left(\frac{2\pi a}{2\pi a + 2l}\right) R_{\text{rad } AS} \tag{39}$$

Finally, the coupling factors as indicated by Eqs. (11) and (12) are

$$\eta_{2js} = R_{2js}/(M\omega) \tag{40}$$

where $j = 1$, 3 and s stands for AF, AS modes, respectively. For nonradiation modes, the radiation is negligible.

Loss Factors

For structural damping, we consider a linear standard solid and ν_e close to 0.5. The viscoelastic theory yields[2,10]

$$E_v \cong E\{[1 + i\omega(E'/E)]/(1 + i\omega C')\}, \quad i\omega = \partial/\partial t \tag{41}$$

$$\nu_v \cong \nu_e$$

Then, the equation for the vibration of cylindrical shell in terms of normal modes W_{mn} becomes

$$\{[1 + i\omega(E'/E)]/(1 + i\omega C')\}\omega_{mn}^2 W_{mn} + \partial^2 W_{mn}/\partial t^2 = 0 \tag{42}$$

This actually means

$$\omega_{mn}^2 W_{mn} + (E'/E)\omega_{mn}^2\, \partial W_{mn}/\partial t + \partial^2 W_{mn}/\partial t^2 + C'\partial^3 W_{mn}/\partial t^3 = 0 \tag{43}$$

To get an effective damping, let the solution be

$$W_{mn} = e^{(i\omega - \delta)t}$$

Then, for small damping, δ

$$\beta_{mn} \cong 2\delta = \left[\left(\frac{E'}{E} - C'\right)\omega_{mn}^2/[1 + (C')^2\omega^2]\right] \tag{44}$$

As a result, the logarithmic decrement is

$$\delta_{\text{dec}} = (2\pi\delta/\omega)_{\omega=\omega_{mn}} = \pi\Delta_1\omega_{mn}/(1 + C\omega_{mn}^2) \tag{45}$$

where

$$\Delta_1 = (E'/E) - C', \quad C = (C')^2$$

Logarithmic decrements were measured for our shell in air, results of which are shown in Fig. 4. Matching of the theoretical and experimental logarithmic decrements at $f = 200$ Hz and $f = 4000$ Hz yields

$$\Delta_1 \cong 5.33 \times 10^{-6} \text{ (sec/rad)}$$

$$C = 2.28 \times 10^{-7} \text{ (sec/rad)}^2$$

The theoretical curve of Fig. 4 was then computed by using these values in Eq. (45).

Since only resonant modes in the narrow frequency band are needed in the prediction, $\omega_{mn} \cong \omega$, the effective damping coefficient for all modes in the frequency band center at ω is approximately

$$\beta_s \equiv \beta_2 = 2\delta = \Delta_1\omega^2/(1 + C\omega^2) = \left(\frac{E'}{E} - C'\right)\omega^2/[1 + (C')^2\omega^2],$$

$$s = AF, AS, NR, \text{ respectively.}$$

The loss factor η_s is then

$$\eta_s = \eta_2 = \beta_s/\omega \tag{46}$$

as it should be.

For air damping, an empirical attenuation factor is given as $e^{-\alpha_A x}$, where¶

$$\alpha_A \cong (f/1000 \text{ Hz})^{3/2}\, 0.085/(20 + \phi_T) \quad \text{ft}^{-1} \tag{47}$$

The frequency f is in Hz and

$$\phi_T = \phi_{20}(1 + 0.067)\,\Delta T \text{ (nondimensional)}$$

ϕ_{20} is the relative humidity at 20°C and ΔT the temperature difference from 20°C. Since Eq. (47) is insensitive to small differences in temperature and humidity, we have taken $\Delta T \cong 0$ and $\phi_{20} = 0.5$; thus, the denominator is approximately 20.5.

A one-dimensional theory is used to determine the damping coefficient as

$$\beta_a \cong 2c_0\alpha_A$$

Therefore, the loss factor in air is

$$\eta_3 = \eta_a = \beta_a/\omega \cong 2\alpha_A\, c_0/\omega \tag{48}$$

Results and Discussion

In effect, results for structural damping have already been presented in Fig. 4. This, of course, was desirable for describing the method utilized to determine material constants. However, at this point, it is appropriate to discuss some of its limitations. As can be seen in Fig. 4, considerable scatter resulted in the experimental data. Such scatter occurs with either method used to determine damping. With the free-decay method, scatter results from nonuniformity of decay curves which is caused by the beating of modes in proximity to each other. On the other hand, with the half-bandwidth technique, an erroneous damping usually results from the spatial shifting about of modal patterns, as well as coupling between nearby modes. With a fixed point for response observation, spatial shifts of modal pattern with frequency have a strong influence on the damping estimate.

Figure 5 presents the system energy distribution obtained by means of the percentage method only, and is useful for studying some details of the statistical energy method. These results are purely theoretical and include the assumption of an ideal $\frac{1}{3}$-octave filter. On the other hand, response

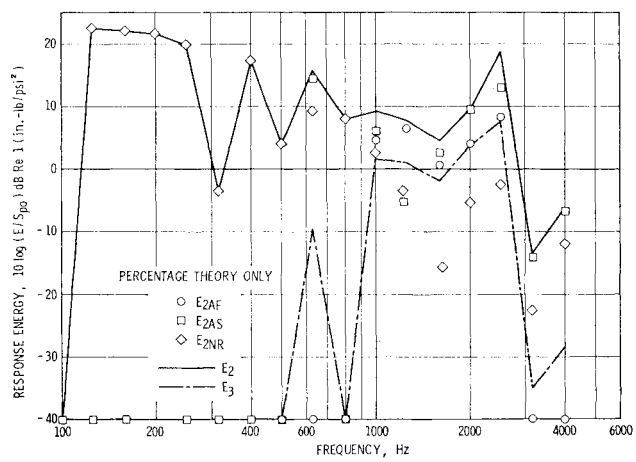

Fig. 5 Energy distribution for system

¶ The unit should be 1/ft instead of db/ft to be consistent with Fig. 3d-3 of Ref. 11.

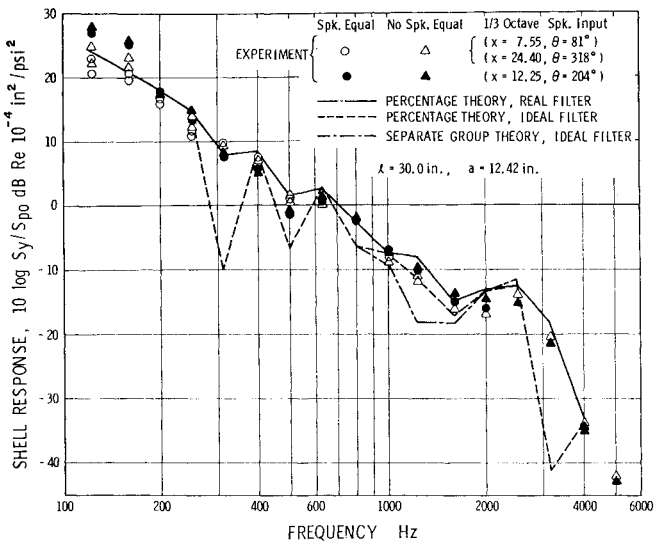

Fig. 6 Shell response ratio.

results for cylinder displacement and interior air cavity can more readily be compared with measured values. Correlations for these parameters are shown in Figs. 6 and 7. In these figures, the dashed theoretical curves (for both separate group and percentage methods) are based on the assumption of an ideal rectangular $\frac{1}{3}$-octave filter, the solid lines represent theoretical curves (for percentage method only) which have been corrected for the real filter characteristic, while multiple experimental values are given at the various frequencies. In Fig. 6, measurements are shown for three different observation points for broadband equalized excitation through 2500 Hz, and $\frac{1}{3}$-octave excitation throughout the entire frequency range. In Fig. 7, the pressure measurements represent maximum and minimum values observed along the centerline of the cylinder, as well as the absolute maximum or minimum value measured anywhere in the tank, for $\frac{1}{3}$-octave excitation in the respective frequency band.

The four basic Eqs. (11–14) for the percentage method were solved simultaneously to determine the four unknown responses E_{2AF}, E_{2AS}, E_{2NR}, and E_3 in terms of the reference excitation power spectral density S_{P_0}. The results are then plotted as in Fig. 5. Subsequent use of Eqs. (21) and (22) then allowed a determination of the response ratios as they appear in Figs. 6 and 7. Similar calculations are performed for the separate group method, except that Eqs. (6–9) are used as the governing equations instead.

A matrix inversion scheme on a digital computer was used for the above solution. Several comments must be made to clarify some of the details of this procedure. Calculation of input power coefficients requires the evaluation of joint acceptance functions by means of Eqs. (28) and (30). A numerical integration scheme employing a mesh size of 0.4 in. was used for this purpose. Further, identification of specific wave numbers, m and n, for each of the modes in the respective $\frac{1}{3}$-octave bands also had to be included. This identification, along with a mode count, was done from the modal diagram in Fig. 4. All computations then included several parameters which were based on some form of $\frac{1}{3}$-octave average value, which was usually a value determined at the band center frequency. These were: 1) spatial correlation of excitation pressure; 2) viscoelastic structural damping; 3) air damping coefficients; 4) radiation coupling factors; and 5) modal density of interior air cavity.

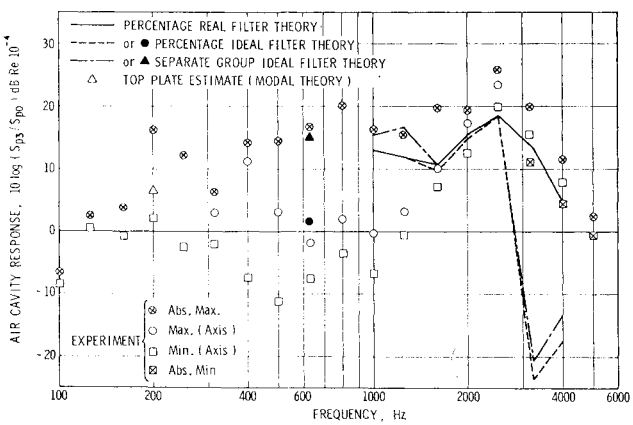

Fig. 7 Air cavity response ratio.

It is interesting to look at the results of Fig. 5 with one major assumption of the percentage method in mind. In particular, the respective energies were combined with the modal densities to provide corresponding energy densities per mode. It was found that the assumptions of Eq. (10) were not very well satisfied by the final results. Nevertheless, the over all comparison of theoretical and experimental results for the percentage method is still quite good, and is better than that for the separate group method. This apparent contradiction simply emphasizes the dire need of further study in the application of the statistical energy method.

It must be borne in mind that the theoretical results represent space-averaged values. Measured results in Fig. 6, which are taken at three rather arbitrarily selected points on the cylinder, indicate that the shell displacement response becomes reasonably uniform in space only for frequencies above 300 Hz. This, then, is the most practical frequency region where use of the statistical energy method becomes appropriate for the cylinder. That is, the actual response values at any point on the tank do not deviate appreciably from the average values, so that predicted values are of practical use. On the other hand, uniformity of air pressure in the three-dimensional interior air space never approaches that experienced by the cylinder, and only settles down to about a 6-db spread above 2000 Hz. It appeared in this case that a measurement of maximum and minimum pressures was more useful than some average value since such an extreme spread is experienced throughout most of the frequency range. Consequently, theoretical values which represent a spacewise average should fall within the spread at all points. This does not occur near 2500 Hz. Thus, each part of the cylinder and air system independently reaches a state of relatively uniform spatial response, which corresponds to a diffuse sound field. This result is probably influenced to some extent by the nondiffuse spatial distribution of the excitation.

The results from the separate group and percentage method (both based on an ideal filter) can readily be compared in Figs. 6 and 7. For the shell response, the two methods give identical results except between about 630 and 2500 Hz. This is to be expected since no radiation occurs outside this range. However, within this range, the percentage method can be seen to provide a better comparison with experimental results. Similar behavior is apparent in the interior pressure response. Except for the single point at 630 Hz, the interior air pressure should be negligible below 1000 Hz since only nonradiating modes occur below this frequency, unless significant nonresonant response is present. However, significant pressures with wide scatter obviously do occur. An attempt at explaining these observed pressures by possible nonresonant response proved to be futile. Additional investigations showed that this discrepancy results from significant resonant vibration of the end baffles and plates, which was neglected in the analysis. One response point based on modal theory allowing for the plate motion at 200 Hz, is shown in Fig. 7 to fall within the measured range.

References

[1] Kana, D. D., "Response of a Cylindrical Shell to Random Acoustic Excitation," *AIAA Journal*, Vol. 9, No. 3, March, 1971, pp. 425–431.

[2] Kana, D. D., Chu, W. H., and Bessey, R. L., "The Response of Cylindrical Shells to Random Acoustic Excitation Over Broad Frequency Ranges," Final Rept., Contract NAS8-21479, Sept. 1970, Southwest Research Institute, San Antonio, Texas.

[3] Manning, J. E. and Maidanik, G., "Radiation Properties of Cylindrical Shells," *Journal of the Acoustical Society of America*, Vol. 36, No. 9, Sept. 1964, pp. 1691–1698.

[4] Arnold, R. N. and Warburton, G. B., "The Flexural Vibrations of Thin Cylinders," *Journal & Proceedings of the Institution of Mechanical Engineers, (London)*, Vol. 167, 1953, pp. 62–74.

[5] Bozich, D. J. and White, R. W., "A Study of the Vibration Responses of Shells and Plates to Fluctuating Pressure Environments," CR 1515, March 1970, NASA.

[6] Lyon, R. H. and Maidanik, G., "Power Flow Between Linearly Coupled Oscillators," *Journal of the Acoustical Society of America*, Vol. 34, No. 5, May 1962, pp. 623–639.

[7] Maidanik, G., "Response of Panels to Reverberant Acoustic Fields," *Journal of the Acoustical Society of America*, Vol. 34, No. 6, June, 1962, pp. 809–826.

[8] Crocker, M. J. and Price, A. J., "Sound Transmission Using Statistical Energy Analysis," *Journal of Sound Vibration*, Vol. 9, No. 3, March 1969, pp. 469–486.

[9] Lyon, R. H., "Noise Reduction of Rectangular Enclosures with One Flexible Wall," *Journal of the Acoustical Society of America*, Vol. 35, No. 11, Nov. 1963, pp. 1791–1797.

[10] Boley, B. A. and Weiner, J. H., *Theory of Thermal Stress*, Wiley, New York, 1960.

[11] Beranek, L. L., "Acoustic Properties of Gases," *Handbook of Physics*, American Institute of Physics, McGraw-Hill, New York, 1963, pp. 3-59–3-70.

MARCH 1972 J. SPACECRAFT VOL. 9, NO. 3

Synthesis of Stiffened Conical Shells

W. A. THORNTON*

Clarkson College of Technology, Potsdam, N.Y.

The development of a method to effect the automated minimum weight design of ring and stringer stiffened shells is presented. Membrane theory is used for the shell prebuckling analysis. The buckling analysis is based upon an arbitrary shell of revolution computer program. The structural analysis includes both buckling and yielding modes of failure. The synthesis involves the coupling of an exterior penalty function with a method for the unconstrained minimization of a function comprised of a sum of squares. Results of the application of the method to the design of the Viking Aeroshell cone are presented. The least weight Viking Aeroshell appears to be an all magnesium shell with ring stiffeners of hollow circular cross section. Because the method incorporates a general shell of revolution buckling analysis, it can be readily modified and applied to the design of any axisymmetrically loaded uniformly stiffened shell of revolution for which a membrane prebuckling solution exists.

Nomenclature

a,b = dimensions of rectangular plate in θ and ξ directions
A = area of stiffener
C,K,D = shell stiffness matrices
d = diameter or web height of stiffener
E = Young's modulus
$f_i(\mathbf{x}),\phi_i(\mathbf{x})$ = constraints
G = shear modulus
H = J^TJ
i = stiffener location parameter
I = stiffener area moment
J = Jacobian matrix
$\tilde{K},\bar{K}$ = stiffness and prebuckling matrices
l = length of shell wall
$\mathbf{M},\mathbf{N}$ = moment and force resultants
n = circumferential mode number
p = uniform pressure (positive for external pressure)
P = axial load (positive for compression)
r = perpendicular distance from shell axis to meridian
R = shell radius
S = stiffener spacing
t = thickness parameter
u_ξ,u_θ,w = displacements of shell middle surface
W = weight of shell
$\mathbf{x}$ = vector of design variables
Y = yield stress
$\mathbf{Z}$ = eigenvector for general shell buckling
α = cone half angle
β,δ,η = shell loading parameters
ε = stiffener eccentricity
$\boldsymbol{\varepsilon},\boldsymbol{\varkappa}$ = extensional and bending strains
λ = loading parameter
ν = Poisson's Ratio
ξ,θ = meridional and circumferential coordinates
ρ = weight density
$\boldsymbol{\sigma},\boldsymbol{\psi}$ = vectors in penalty function method
$\boldsymbol{\tau}$ = stress vector
$\phi_\xi,\phi_\theta,\phi$ = rotations of normal to shell middle surface
Φ = penalty function

Subscripts

a,b = actual and buckling value
R,S = ring and stringer quantities
t = stiffener torsional properties
W = wall quantities

Received July 6, 1971; revision received November 9, 1971. Supported by NASA Research Grant NGL-33-007-075.

Index category: Optimal Structural Design.

* Assistant Professor of Civil Engineering. Member AIAA.